Phase-shifting laser diode Sagnac interferometer for surface profile measurement

Takamasa Suzuki*, Masato Shirai, and Osami Sasaki

Niigata University, Faculty of Engineering
8050 Ikarashi 2, Niigata City, 950-2181, Japan

ABSTRACT

A phase-shifting Sagnac interferometer that uses wavelength tunability of the laser diode is proposed. A Sagnac interferometer itself is robust for the mechanical disturbances because it has a common path configuration and requires no special reference. Unbalanced optical path introduced between p- and s-polarized beams enables us to implement easy phase-shift by the direct current modulation. Several experimental results indicate that the proposed system is useful for the disturbance-free precise measurement.

Keywords: laser diode, Sagnac interferometer, phase-shift, surface profile measurement

1. INTRODUCTION

Precise measurement is critical at all stages of high-tech manufacturing process. Optical interferometers are suitable and convenient for such purposes on account of non-contact method and few nanometers of resolution. The common interferometers such as Michelson-, Twyman-Green-, and Mach-Zehnder- interferometers have been used to measure various optical parts on an optical bench. In a workshop, however, mechanical disturbance does not bring their ability into full play, even though they have extremely high resolutions. Many techniques have been proposed to reduce the effect of the external disturbance. Stroboscopic data-acquisition technique allows us to capture clear images and it is effective especially for the observation of a moving object. Most of them, however, require some special optical devices. The pulsed digital holographic interferometer has measured rotating objects by using Q-switched ruby laser[1]. Although stroboscopic phase-shifting interferometer measures high-speed surface deformation, it employs Q-switched Nd:YAG and special point diffraction plate (PDP)[2]. A modified Michelson interferometer that simultaneously captures three phase-shifted interferograms by a single CCD camera uses special diffraction grating[3]. A differential detection and/or a feedback technique are also available to the disturbance elimination. In the former technique, the phase difference between the reference point and the measuring point on the object gives us the disturbance eliminated surface profile[4]. On the other hand, wavelength of a laser diode (LD) is modulated by varying the injection current. When this wavelength tunability is combined with the electrical feedback loop, in the latter technique, the small mechanical disturbance is dramatically reduced[5-7]. Although these techniques do not require any special optical component, the performance of the disturbance elimination is restricted by the amplitude of the external disturbance. From this point of view, optical arrangement that is, in itself, robust for the disturbance is necessary to cope with such disturbance of large amplitude.

The system we propose in this paper employs a Sagnac interferometer and wavelength tunability of the LD. a A Sagnac interferometer has been investigated for long time[8] and used for many applications in different configurations[9-11]. Above all, because a Sagnac interferometer has a common path configuration and self-reference nature, optical setup itself is robust for the external disturbance. In this arrangement, we have one problem in phase-shifting under the current modulation, because the optical path difference (OPD) of the Sagnac interferometer is zero. To overcome this problem, OPD is intentionally introduced into the optical setup. We demonstrated the surface profile measurement by use of current modulation of the LD.

*takamasa@eng.niigata-u.ac.jp; phone / fax : +81-25-262-7215;

Advanced Materials and Devices for Sensing and Imaging III, edited by Anbo Wang, Yimo Zhang, Yukihiro Ishii, Proc. of SPIE Vol. 6829, 68290A, (2007)
0277-786X/07/$18 · doi: 10.1117/12.756447

2. PRINCIPLE

We employed polarized Sagnac interferometer, which consists of polarizing beam splitter (PBS), three mirrors (M1, M2, and M3) and two lenses (L1, and L2) as shown in Fig. 1. The laser diode (LD) radiates linear polarized beam whose axis is inclined 45 degrees. The s-polarizing beam first makes round of the Sagnac loop clockwise along the route 1 to 3 (Fig. 1) and focused onto the object through lenses L1 and L2 as shown in Fig. 2. The light reflected from the object is collimated by the lenses L1 and L2 and back-propagates along the route 6 to 8 (Fig. 1). This light reaches to the CCD camera as the reference beam.

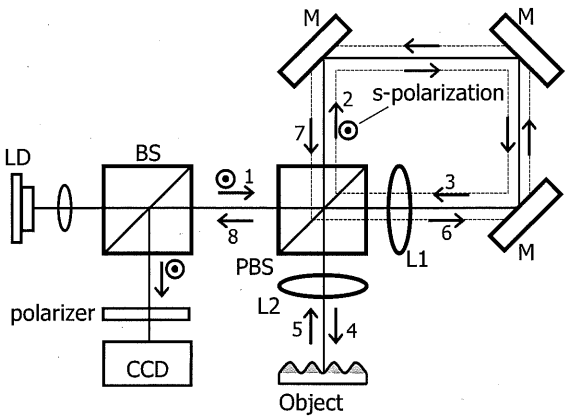

Fig. 1 Optical path of the s-polarizing beam. LD, laser diode; BS, beam splitter, PBS, polarizing beam splitter; M, mirrors; L1and L2, lenses The s-polarizing beam first rounds clockwise and back-propagates counterclockwise after reflecting on the object.

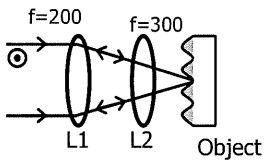

Fig 2 Schematic of the s-polarizing beam. The beam is focused onto the object through lenses L1 and L2.

On the other hand, p-polarizing beam rounds the Sagnac loop counterclockwise along the route 1 to 3 (Fig. 3) and reaches to the object through lenses L1 and L2 as shown in Fig. 4. In this case, the optical path length between L1 and L2 is different from the case of s-polarizing beam. The object is irradiated by the collimated light. The reflected light back-propagates along the route 6 to 8 (Fig. 3) and reaches to the CCD camera as the object beam. The reference beam and the object beam interfere after passing the polarizer. The optical setup itself is robust for the external disturbance because it has a common path structure and also requires no special references.

In the standard four-step algorithm, we capture a series of images represented by

$$S_i(x,y) = a(x,y) + b(x,y)\cos\left[\alpha(x,y) + \alpha_i\right] \quad (\text{i} = 1, 2, 3, 4), \tag{1}$$

where $\alpha(x, y)$ represents the surface profile of the object,

$$\alpha_i = \frac{2\pi L}{\lambda_0^2}\beta k V_i \tag{2}$$

is the phase change introduced by the modulating current V_i. The OPD, the central wavelength, the modulation efficiency of the LD, and the transfer function from voltage to current are represented by L, λ_0, β, and k, respectively. If the condition of

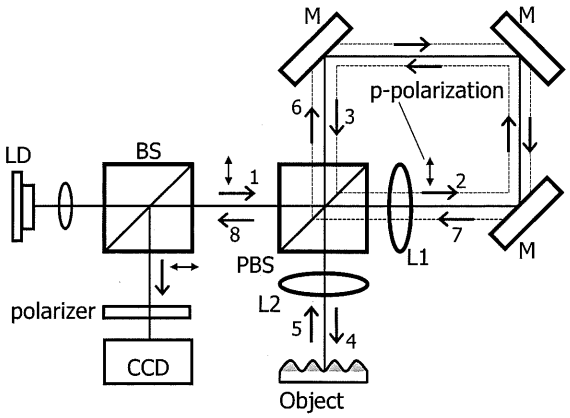

Fig 3 Optical path of the p-polarizing beam. The p-polarizing beam first rounds counterclockwise and back-propagates clockwise after reflecting on the object.

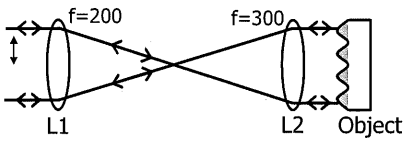

Fig. 4 Schematic of the p-polarizing beam. The beam is collimated onto the object through lenses L1 and L2.

$$\alpha_i = (i-1)\frac{\pi}{2} \tag{3}$$

is realized by regulating I_i, we can get the phase-shifting images required for the calculation of surface profile. A well-known phase-shifting formula is given by

$$\alpha(x,y) = \tan^{-1}\left[\frac{S_4(x,y) - S_2(x,y)}{S_1(x,y) - S_3(x,y)}\right]. \tag{4}$$

Equation (2) shows that we have to intentionally introduce the OPD into the optical setup, because the OPD of the Sagnac interferometer is zero as it is.

The system we propose in this paper is shown in Fig. 5. The OPD introducing system (OPD-IS) is placed between the laser source and the Sagnac interferometer. It is composed of two PBSs (PBS2 and PBS3) and two mirrors (M4 and M5). The s- and the p-polarizing beam are split once at PBS2 and combined at PBS3 again. Since the s-polarization propagates longer path than the p-polarization, we can introduce OPD between the s-polarizing beam and the p-polarizing beam.

3. EXPERIMENTAL SETUP

Schematic of the experimental setup is illustrated in Fig. 5. The laser beam irradiated from the LD passes the optical isolator and is expanded by the beam expander. This laser beam incidents on the interferometer after passing OPD-IS and forms interferogram on the CCD camera. The phase modulated interferograms are processed by the computer (PC) so as to obtain the surface profile. The video signal is also sent to the phase-shifting signal generator (PSSG), which generates the phase-shifting signal and the synchronous (Sync) signal. The PC captures the interferograms synchronized with the Sync signal.

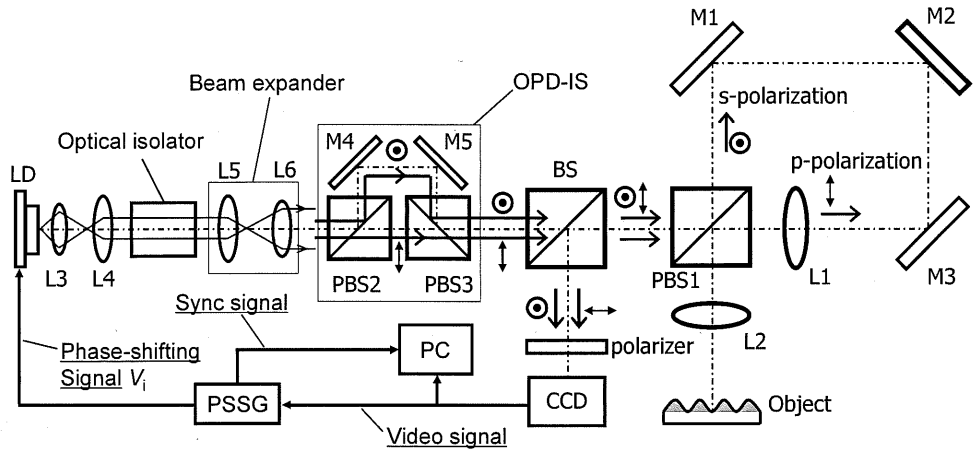

Fig. 5 Schematic of the experimental setup. OPD-IS, optical path difference introducing system; PC, computer; PSSG, phase-shifting signal generator. The s-polarizing beam and the p-polarizing beam are once divided at the OPD-IS so as to introduce unbalanced optical path. The polarizer in front of the CCD camera forms interference fringe. The phase-shifting signal is generated synchronized with the video signal

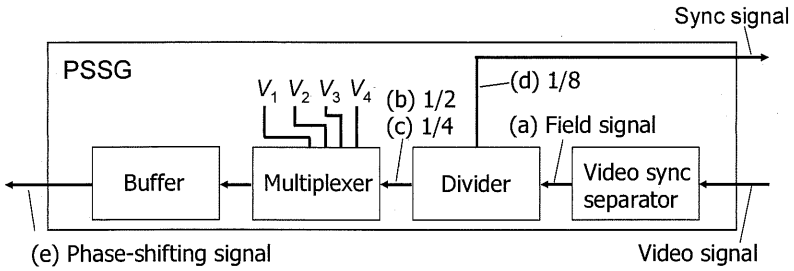

Fig. 6 Block diagram of the PSSG. The video sync separator separates the synchronous signal so called a field signal from the video signal The divider decreases the frequency of the field signal by the factor of 2, 4, and 8 One of the phase-shifting signals V_1, V_2, V_3, and V_4 is selected by the multiplexer and injected into the LD.

Block diagram and the timing chart of the PSSG are shown in Figs. 6 and 7, respectively. The video sync separator extracts the field signal, which indicates the even and odd lines in the NTSC standards. The field signal is divided by 2, 4, and 8 with the frequency divider. The multiplexer selects one of the phase-shifting signals V_1, V_2, V_3, and V_4 by means of the combination of 1/2 and 1/4 signals. The output signal of the multiplexer is buffered and fed into the LD as the phase-shifting signal (Fig. 7(e)). The signal of 1/8 is used as the Sync signal. Overview of the setup is shown in Fig. 8. It is constructed on the iron plate place on the wooden desk.

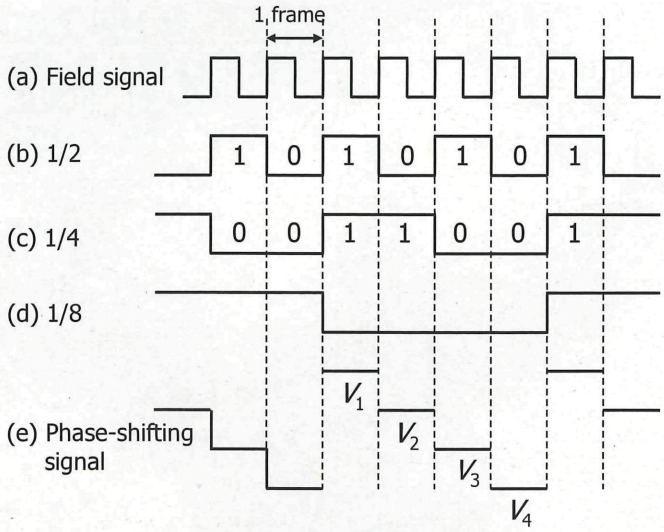

Fig. 7 Timing chart of the PSSG. The divider decreases the frequency of (a) the field signal by (b) 1/2, (c) 1/4, and (d) 1/8. The level V_1, V_2, V_3, and V_4 of (e) the phase-shifting signal is chosen by the combination of the signal (b) and (c).

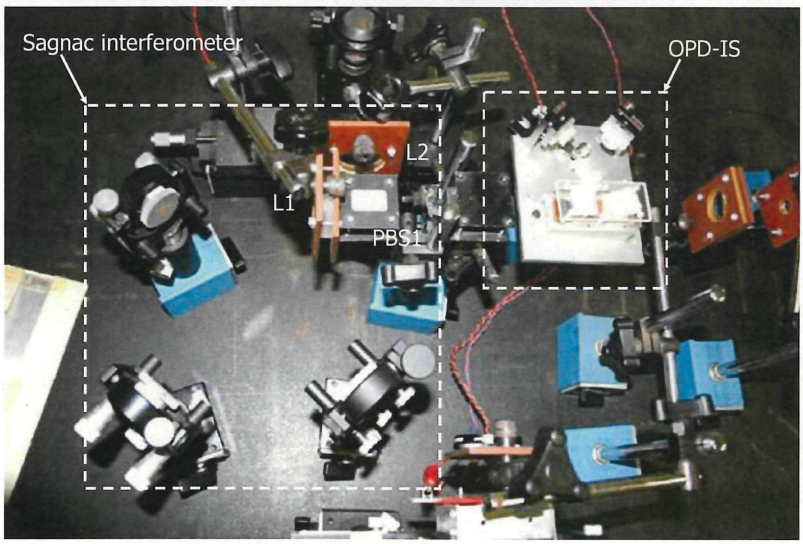

Fig. 8 Photo of the experimental setup.

4. EXPERIMENTS

We first confirmed the robustness of the optical setup in comparison with a Twyman-Green interferometer that is placed on the same iron plate. We put the motor on the iron plate and observed interferograms at the stationary and the rotating state. The interferograms observed with the Twyman-Green and the Sagnac interferometer are clear as shown in Figs. 9(a) and 9(b) if the motor stops. If the motor rotates, however, the fringe in the Twyman-Green interferometer disappeared as shown in Fig. 9(c), while that in the Sagnac interferometer is observed clearly (Fig. 9(d)).

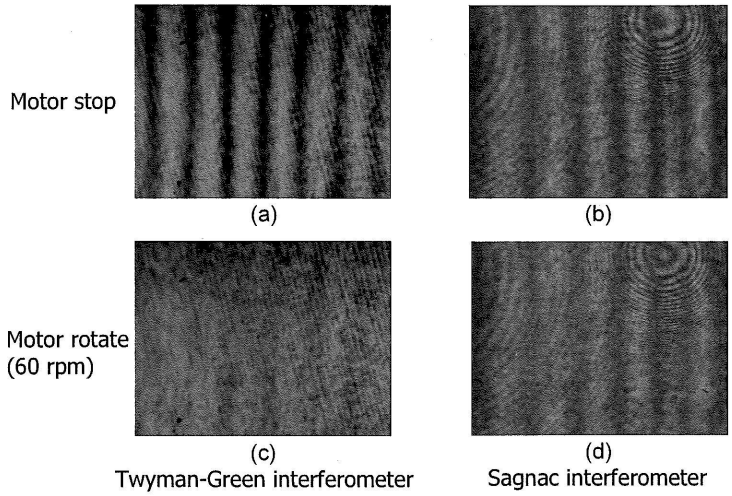

Fig. 9 Interferograms observed by (a) the Twyman-Green interferometer and (b) the Sagnac interferometer when the motor was stationary state. Interferogram was disappeared in (c) the Twyman-Green type when the motor is rotational state, while it remained in (d) the Sagnac interferometer.

Next, we observed the phase distribution given by the interferogram. A flat mirror was used as the object. The original images captured by the CCD camera are shown in Fig. 10.

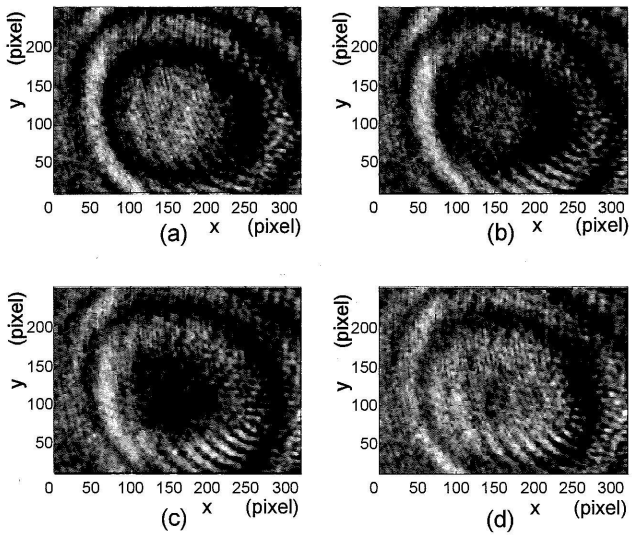

Fig. 10 Captured interferograms whose phase were shifted by (a) 0, (b) $\pi/2$, (c) π, and (d) $3\pi/2$ rad, respectively.

The images shown from (a) to (d) are respectively corresponding to the signals indicated by Eq. (1). The images in the calculating process are displayed in Fig. 11. The images correspond to the numerator and the denominator in Eq. (4) are

shown in Figs. 11(a) and 11(b), respectively. We can find that the phase difference between them is $\pi/2$. The images corresponding to the argument of Eq. (4) and $\alpha(x, y)$ are shown in Figs. 11(c) and 11(d), respectively. A three-dimensional plot of the phase distribution is illustrated in Fig. 12. Although the object was a flat mirror, the obtained profile shows a spherical shape. It is thought that the phase distribution on the reference beam is not flat but spherical. Exact surface profile measurement would be realized if the distortion of the reference beam were removed or subtracting the spherical shape from the measured profile.

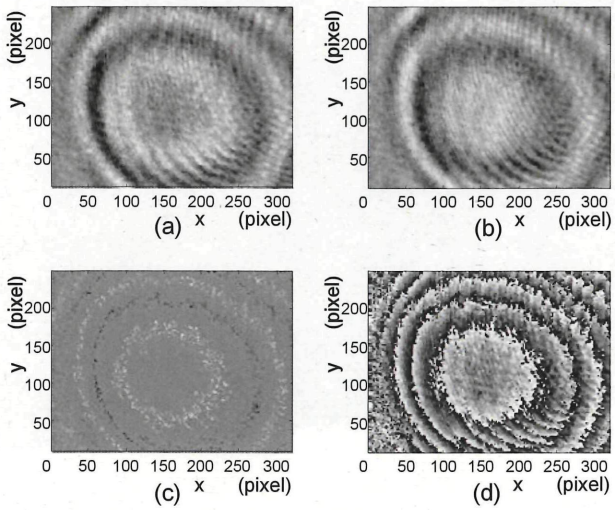

Fig. 11 Processed images corresponding to (a) S_4-S_2, (b) S_1-S_3, (c) $(S_4-S_2)/(S_1-S_3)$, and (d) the phase distribution $\alpha(x, y)$.

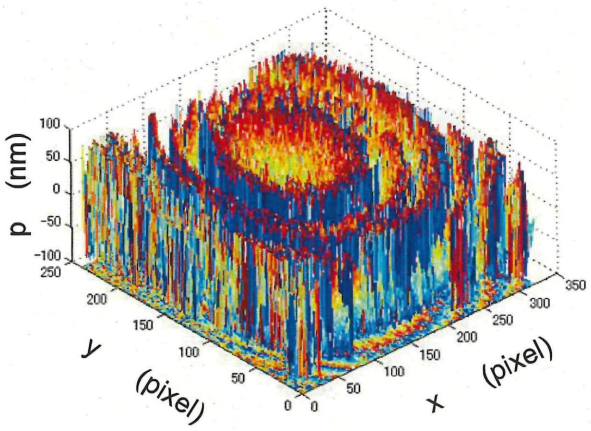

Fig. 12 Three-dimensional plot of the phase distribution.

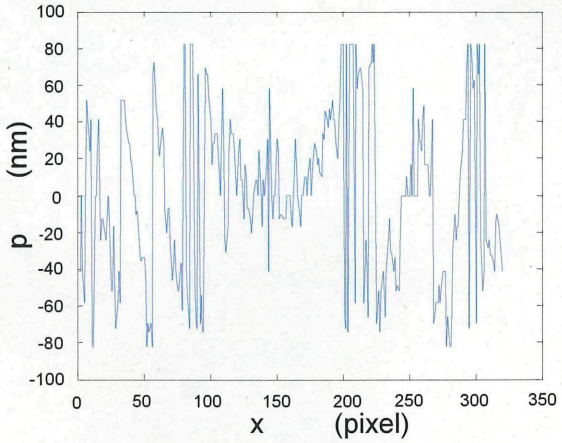

Fig. 13 Sectional profile of the 3-D plot.

REFERENCES

1. C. P.-Lopez, F. M. Santoyo, G. Pedrini, S. Schedin, and H. J. Tiziani, "Pulsed digital holographic interferometry for dynamic measurement of rotating objects with an optical derotator," Opt. & Photo. News 13, S2-S6 (2002).
2. Y. Kwon, D. M. Shough, and R. A. Williams, "Stroboscopic phase-shifting interferometry," Opt. Lett., 12, 855-857 (1987).
3. A. Hettwer, J. Kranz, and J. Schwider, "Three channel phase-shifting interferometer using polarization-optics and a diffraction grating," Opt. Eng., 39, 960-966 (2000).
4. T. Suzuki, O. Sasaki, K. Higuchi, T. Maruyama, "Differential type of phase locked laser diode interferometer free from external disturbance," Appl. Opt., 31, 7242-7248 (1992).
5. T. Yoshino, M. Nara, S. Mnatzakanian, B. S. Lee and T. C. Strand, "Laser diode feedback interferometer for stabilization and displacement measurements." Appl. Opt. 26, 892-897 (1987).
6. O. Sasaki, K. Takahashi, T. Suzuki, "Sinusoidal phase modulating laser diode interferometer with a feedback control system to eliminate external disturbance," Opt. Eng. 29, 1511-1515 (1990).
7. O. Sasaki, H. Sasazaki, T. Suzuki, "Two-wavelength sinusoidal phase modulating laser diode interferometer insensitive to external disturbances," Appl. Opt., 30, 4040-4045 (1991).
8. P. Hariharan, "Sagnac or Michelson-Sagnac interferometer?," Appl. Opt., 14, 2319-2321 (1975).
9. T. Shirai, T. H. Barnes, and T. G. Haskel, "Surface profile measurement by meanes of a polarization Sagnac interferometer with parallel optical feedback," Opt. Lett., 24, 297-299 (1999).
10. D. H. Hurley and O.B.Wright, "Detection of ultrafast phenomenon by use of a modified Sagnac interferometer," Opt. Lett., 24, 1305-1307 (1999).
11. T. Tachizaki, T. Muroya, and O. Matsuda, "Scanning ultrafast Sagnac interferometry for imaging two-dimensional surface wave propagation," Rev. Sci. inst., 77, 043713 (2006).